An all-carbon vdW heterojunction composed of penta-graphene and graphene: Tuning the Schottky barrier by electrostatic gating or nitrogen doping

Yaguang Guo, Fancy Qian Wang, and Qian Wang

Citation: Appl. Phys. Lett. **111**, 073503 (2017);
View online: https://doi.org/10.1063/1.4986604
View Table of Contents: http://aip.scitation.org/toc/apl/111/7
Published by the American Institute of Physics

Articles you may be interested in

Elucidation of luminescent mechanisms of size-controllable $MoSe_2$ quantum dots
Applied Physics Letters **111**, 073105 (2017); 10.1063/1.4999444

Inhomogeneous degradation in metal halide perovskites
Applied Physics Letters **111**, 073302 (2017); 10.1063/1.4999630

Piezoelectricity in two dimensions: Graphene vs. molybdenum disulfide
Applied Physics Letters **111**, 083107 (2017); 10.1063/1.5000496

Enhanced p-type behavior in the hybrid structure of graphene quantum dots/2D-WSe_2
Applied Physics Letters **111**, 111603 (2017); 10.1063/1.4989598

Pulsed laser deposition for the synthesis of monolayer WSe_2
Applied Physics Letters **111**, 073101 (2017); 10.1063/1.4986851

Room temperature quantum spin Hall insulator: Functionalized stanene on layered PbI_2 substrate
Applied Physics Letters **111**, 072105 (2017); 10.1063/1.4985643

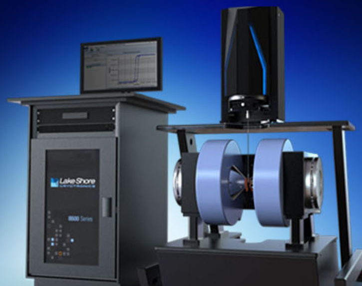
8600 Series VSM
For fast, highly sensitive measurement performance

APPLIED PHYSICS LETTERS **111**, 073503 (2017)

An all-carbon vdW heterojunction composed of penta-graphene and graphene: Tuning the Schottky barrier by electrostatic gating or nitrogen doping

Yaguang Guo,[1,2] Fancy Qian Wang,[1,2] and Qian Wang[1,2,a)]
[1]*Center for Applied Physics and Technology, College of Engineering, Peking University, Beijing 100871, China*
[2]*Collaborative Innovation Center of IFSA (CICIFSA), Shanghai Jiao Tong University, Shanghai 200240, China*

(Received 6 June 2017; accepted 30 July 2017; published online 16 August 2017)

The non-zero band gap together with other unique properties endows penta-graphene with potential for device applications. Here, we study the performance of penta-graphene as the channel material contacting with graphene to form a van der Waals heterostructure. Based on first-principles calculations, we show that the intrinsic properties of penta-graphene are preserved in the heterojunction, which is different from the conventional contact with metal surfaces. The stacked system forms an n-type Schottky barrier (Φ_e) at the vertical interface, while a negative band bending occurs at the lateral interface in a current-in-plane model. From the device point of view, we further demonstrate that a low-Φ_e or an Ohmic contact can be realized by applying an external electric field or doping graphene with nitrogen atoms. This allows the control of the Schottky barrier height, which is essential in fabricating penta-graphene-based nanotransistors. *Published by AIP Publishing.*
[http://dx.doi.org/10.1063/1.4986604]

Last ten years witness the rapid growth of two dimensional (2D) materials.[1] Researches ranging from the basic physics and chemistry to the applications for electronics, energy, and environment demonstrate that 2D materials exhibit very different fascinating properties as compared to their 3D counterparts.[2] Among all, graphene is undoubtedly of great importance due to its superior electronic and mechanical properties,[3–5] which is regarded as the key ingredient for electronic devices in the future. However, the zero-band gap of graphene significantly limits its applications in the semiconductor industry,[6] and there is no controllable way to open the gap while perfectly keeping the fundamental nature of graphene. In this context, extensive efforts have been devoted to exploring other 2D materials that have semiconducting characteristics such as transition metal dichalcogenides (TMDs)[7,8] and layered black phosphorous.[9] Recently, our group predicted a 2D carbon allotrope, penta-graphene (PG), which is entirely composed of carbon pentagons.[10] State-of-the-art calculations showed that penta-graphene exhibits a negative Poisson ratio, an ultrahigh ideal strength, and especially an intrinsic band gap of about 3.25 eV.[10] These properties make penta-graphene a promising alternative to graphene in electronic device applications.

The rise of 2D materials offers a platform for the creation of heterostructures by vertically stacking different 2D sheets together via the van der Waals (vdW) force.[11] Because charge transfer is different with different 2D materials, vdW heterostructures provide an interesting possibility in band structure engineering with applications in tunneling and optoelectronic devices, solar cells, light-emitting diodes, and so on.[11–14] For example, the fabrication of nanotransistors based on 2D materials has been experimentally realized by stacking MoS_2 or hBN on the top of graphene,[15–17] which exhibit excellent performances such as a high on/off ratio and a tunable Schottky barrier height. Theoretically, graphene has been also combined with other 2D semiconductors such as black phosphorous,[18] GaSe,[19] and halide perovskites to form tunnel junctions. In this device paradigm based on vdW heterostructures, 2D semiconductors are considered as the channel materials, while graphene is used as the metallic electrode. Previous studies have demonstrated that unlike conventional metal-semiconductor contacts, the absence of dangling bonds in 2D materials can prevent the strong bonding at the junction interface, hence preserving the intrinsic properties of semiconductors.[18,20] In addition, Fermi level pinning is weakened in such vdW contacts, leading to a tunable Schottky barrier height by using 2D metals with different work functions.[21,22] These advantages are very desirable in transistor applications.

Since penta-graphene possesses a non-zero band gap,[10] it is of great interest to integrate this unique property into an electronic device by constructing a vdW heterostructure via stacking penta-graphene and graphene together and to explore whether the stacked system has some useful electronic properties. In this letter, we systematically study the geometric and electronic structures of an all-carbon vdW heterostructure constructed by penta-graphene (PG) and graphene (G), named PG/G. We first use our in-house code to address the issue of lattice match. Then, we study the interface properties which determine the device performance, including charge transfer, band alignment, and Schottky barrier. We show that the electronic properties of both penta-graphene and graphene are well preserved after being stacked up, and an n-type channel is formed due to the negative bend banding in a current-in-plane (CIP) device. Moreover, we predict that it is possible to tune the Schottky barrier height by applying an external

[a)]Electronic mail: qianwang2@pku.edu.cn

TABLE I. Lattice parameters of the penta-graphene and graphene supercells. The lattice constants and the angle between the vectors are in the unit of angstrom and degree, respectively. The last column shows the total number of atoms in the heterostructures.

	Penta-graphene $a=b=3.64$Å, $\alpha=90°$			Graphene $a=b=2.46$Å, $\alpha=120°$			Mismatch (%)			Number of atoms
	u_1	v_1	γ_1	u_2	v_2	γ_2	u_{1_2}	v_{1_2}	γ_{1_2}	
Case 1	7.38	25.57	90.00	7.28	25.48	90.00	1.37	0.33	0.00	156
Case 2	15.00	16.28	77.47	14.96	16.13	77.70	0.30	0.91	0.29	198
Case 3	15.00	18.56	87.27	14.96	18.57	88.13	0.30	0.07	0.97	232
Case 4	16.28	18.56	74.75	16.13	18.57	74.18	0.91	0.07	0.77	242
Case 5	13.12	23.31	85.03	13.02	23.47	84.32	0.82	0.68	0.85	254

electric field to the heterostructure or doping the graphene layer with N atoms.

Our first-principles calculations within the framework of the density functional theory (DFT) are carried out using the Vienna *Ab-initio* Simulation Package (VASP)[23,24] employing the projector augmented wave (PAW) pseudopotentials[24,25] and the Perdew-Burke-Ernzerhof (PBE) exchange-correlation functional.[26] To correctly describe the effect of the vdW interactions, we employ a dispersion-corrected DFT method (optB88-vdW).[27,28] The plane-wave cutoff energy is 500 eV for all the calculations. The Brillouin zone is sampled with $11 \times 1 \times 1$ Monkhorst-Pack special *k*-point meshes.[29] The systems are fully relaxed until the final force on each atom is less than 0.01 eV/Å. Work functions are calculated by subtracting the corresponding electronic levels with respect to the vacuum level in the supercell.

Unlike graphene/hBN (Ref. 12) and MoS_2/WS_2 (Ref. 30) heterostructures, which can be directly stacked together because of the small lattice mismatch between their primitive cells, the lattice shapes of penta-graphene and graphene are very different from each other (see Table I). Therefore, special care is needed in the construction of the heterostructure model that the lattice mismatch strain should be minimized. To this end, we use our in-house lattice-match code to construct the supercell model. In this code, we implement an approach based on the work by Zur and McGill's,[31] which can render reasonable supercell models that are amenable to DFT calculations. We look for the lattice match based on the interface area. For a certain area, we use a mathematical method to find all the shapes of the superlattice, and by comparing three lattice parameters (u, v, and γ) one by one, we search the best match between them. We set the mismatch of the lattice parameters (u, v, and γ) between the penta-graphene and graphene superlattices to be less than 2% to insure that the lattice strain is negligible (see Table I). Given that DFT calculations cannot hold a very large system, we also set the total number of atoms in the system less than 300 at the same time.

Table I lists the lattice parameters of the penta-graphene (u_1, v_1, and γ_1) and graphene supercell (u_2, v_2, and γ_2) by using the lattice-match code. One can see that u_1, v_1, and γ_1 are close to u_2, v_2, and γ_2, respectively, and therefore, the two supercells can be stacked together with minor lattice mismatch. We also find that the way to match two carbon sheets is not unique, where there are five possible models that meet the requirements set in the code. We choose Case 1 as the candidate [see Fig. 1(a)] because it contains minimum atoms so that the system can be dealt easily in calculations. Note that, in our simulation, we slightly stretch the penta-graphene supercell (u_1, v_1, and γ_1) to match the fixed graphene supercell (u_2, v_2, and γ_2) when stacking them together and then optimize the heterostructure without any constrains of atomic coordinates. More details about constructing the heterostructure can be seen in the supplementary material.

Figure 1(a) shows the fully optimized PG/G heterostructure. We note that after optimization, both the penta-graphene and graphene layers remain intact without any obvious geometric changes, implying that lattice strain is indeed negligible in this heterostructure model. We then characterize the interface stability by using the binding energy defined by $E_b = (E_{PG/G} - E_{PG} - E_G)/n$, where $E_{PG/G}$ is the total energy of the PG/G heterostructure, E_{PG} and E_G are the total energies of the freestanding penta-graphene and graphene sheet, respectively, and n represents the number of carbon atoms in the graphene layer. Figure 1(b) shows the binding energy as a function of the interlayer distance between the penta-graphene and graphene layers. We find that the equilibrium distance is 3.14 Å with a binding energy of 56 meV (absolute value) per carbon atom. Compared with other van der Waals crystals,[32]

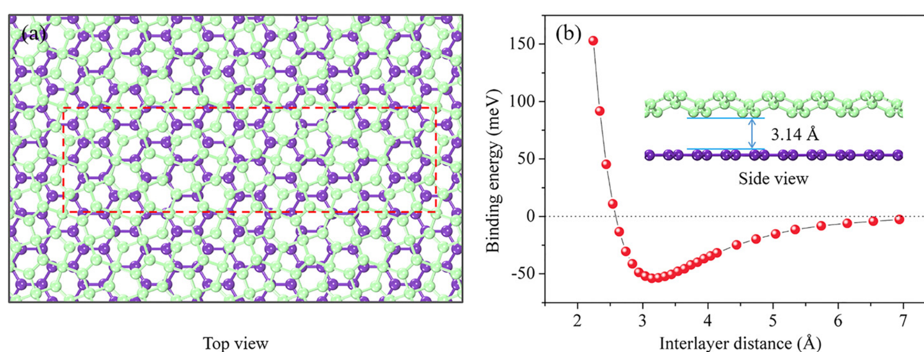

FIG. 1. (a) Top view of the optimized PG/G heterostructure. The red dashed line represents the crystal lattice of the heterostructure. (b) Binding energy as a function of the interlayer distance between penta-graphene and graphene. The inset image shows the side view of the equilibrium heterostructure. Green and purple balls represent the carbon atoms in penta-graphene and graphene, respectively.

such as graphite [$d = 3.33$ Å and $E_b = 52$ meV], hexagonal boron nitride [$d = 3.33$ Å and $E_b = 65$ meV], and phosphorene on graphene [$d = 3.45$ Å and $E_b = 60$ meV], both the interlayer distance and binding energy have the same order of magnitude as those of the typical van der Waals crystals, implying that the PG/G heterostructure can be classified into the category of van der Waals type.

We then check the thermal stability of the PG/G heterojunction by performing *ab initio* molecular dynamics (AIMD) simulations using a canonical (NVT) ensemble. The simulations are carried out with a Nosé thermostat[33] at 300 K for 10 picoseconds (ps) with a time step of 1 femtosecond (fs). The fluctuation of the total energy with simulation time is plotted in Fig. S2 in the supplementary material. After 10 000 steps, no obvious distortion is observed in the structure, and the average value of the total energy remains nearly constant during the entire simulation. This implies that the PG/G heterojunction is thermally stable up to at least 300 K.

We first examine the electronic structure of the PG/G heterojunction. For the convenience of comparison, we use the superlattice instead of the unit cell to calculate the band structures. The electronic band structures of freestanding penta-graphene and graphene are given in Fig. S3 in the supplementary material. All of our results are in good agreement with previous studies.[10,34] We note that the valence band maximum (VBM) and the conduction band minimum (CBM) of penta-graphene, as well as the Dirac point of graphene, are all located between the Γ and X points in the Brillouin zone. Therefore, we focus on the k-path from the Γ to the X point of the band structure in the remaining discussions. The calculated projected band structures of the PG/G heterojunction on penta-graphene and graphene are plotted in Figs. 2(a) and 2(b), respectively, which clearly show that the electronic structures of both penta-graphene and graphene are well preserved after being stacked together, consistent with the important feature of vdW contacts.[18] However, a close inspection uncovers that the valence band edge of penta-graphene is mixed with some deep states of graphene, which induces an additional hybridized state in the electronic structure of penta-graphene, as shown in Fig. 2(c). Our previous study demonstrated that the VBM of penta-graphene is contributed by the p_z orbitals of the sp^2-hybridized carbon atoms,[10] and thus, this hybridization is solely from the interaction between the p_z orbitals of penta-graphene and the π cloud of graphene.

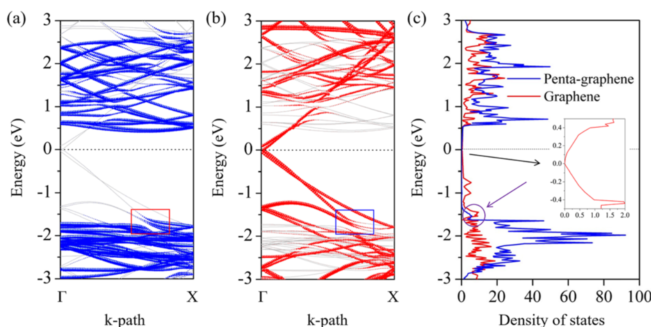

FIG. 2. Band structure of the PG/G heterojunction projected on (a) penta-graphene and (b) graphene. (c) Partial density of states of penta-graphene and graphene in the PG/G heterostructure. The Fermi levels are shifted to zero.

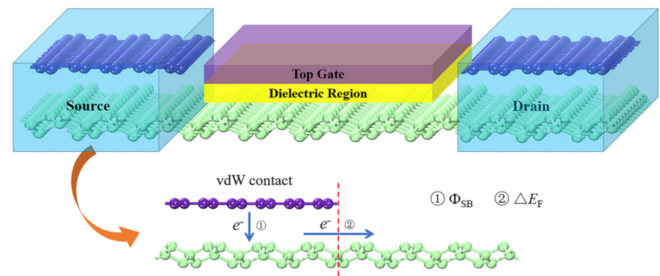

FIG. 3. The schematic diagram of a PG/G heterojunction based transistor. Φ_{SB} and ΔE_F represent the Schottky barrier and band bending, respectively.

Next, we make a contact evaluation for this heterostructure from the device point of view. Figure 3 shows the schematic diagram of a PG/G heterojunction based transistor. In general, charge carriers moving from the electrode to the channel need to overcome two energy barriers at two interfaces (as labeled in Fig. 3).[35] One appears at the lateral interface (band bending, ΔE_F), which is between the heterojunction and the freestanding channel part. The other one is at the vertical interface in the contact (Schottky barrier, Φ_{SB}), which determines the efficiency of carrier injection from the metal to the semiconductor.

At first, we use a current-in-plane (CIP) model[36] to calculate the band bending in the PG/G heterojunction as plotted in Fig. 4. The CIP system is composed of three parts: the left is the PG/G heterostructure, while the right part is the freestanding penta-graphene sheet, and the interface is in the middle. Due to the difference in work functions of the metal and semiconductor, there is a band bending at the interface, which can be estimated by the Fermi level difference (ΔE_F), i.e., $\Delta E_F = W_{PG/G} - W_{PG}$, where $W_{PG/G}$ and W_{PG} are the work functions of the PG/G heterostructure and freestanding penta-graphene, respectively. In Fig. 4, we can see that the calculated $W_{PG/G}$ is 4.53 eV, W_{PG} is 6.16 eV, consequently,

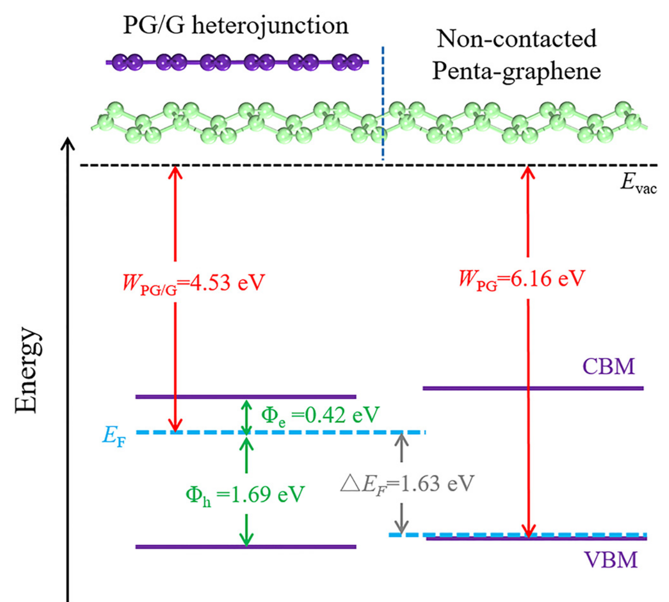

FIG. 4. Schematic plot of a CIP model and band alignment. $W_{PG/G}$ and W_{PG} are the work functions of the PG/G heterostructure and single-layer penta-graphene, respectively. E_{vac} represents the vacuum level that all the values are aligned.

the band bending (ΔE_F) is about -1.61 eV. Since $\Delta E_F < 0$, the electrons will move from the PG/G heterostructure to the freestanding penta-graphene, leading to an n-type channel, hence making the CIP device n-type without further doping. The results are different from those of the heterostructure of graphene and phosphorene, which predicts a p-type contact.[18]

Next, we discuss the Schottky barrier in the PG/G heterojunction, the most important parameter that determines the contact resistance in a transistor device.[37] The Schottky barrier height (Φ_{SB}) is defined as the energy difference between the Fermi level and the band edge of the semiconductor in a heterostructure

$$\Phi_e = E_{CBM} - E_F, \quad \Phi_h = E_F - E_{VBM}, \tag{1}$$

where Φ_e and Φ_h are the Φ_{SB} values for electrons and holes, respectively, E_F represents the Fermi level, while E_{CBM} and E_{VBM} denote the energy of the CBM and VBM of the semiconductor in the heterostructure, respectively, which are identified from atom projected density of states. From Figs. 2(a) and 4, we obtain a Φ_{SB} value of 0.42 eV for electrons and 1.69 eV for holes in the PG/G heterostructure. The Fermi level is near the edge of the conduction band of penta-graphene, indicating an n-type Schottky barrier with electrons as the major transport carriers. For device applications, it is better to get a smaller Schottky barrier height or even induce an Ohmic contact to reduce the contact resistance. It has been demonstrated that Schottky barriers can be tuned by applying a perpendicular external electric field.[18,38,39] Here, we apply the same method to the PG/G heterojunction. In Fig. 5(a), we plot the evolution of the Schottky barrier heights subject to a positive and a negative electric field. Without the field, the system shows an n-type Schottky barrier as Φ_e is less than Φ_h. By applying a positive field, we find that the Fermi level gets closer to the valence bands as the field strength increases, leading to a reduction in Φ_h and an increase in Φ_e. Note that Φ_h becomes smaller than Φ_e when the field strength reaches 5 V/nm, implying that the Schottky barrier transforms from the n-type to the p-type. On the contrary, the negative field makes the Fermi level moves towards the conduction bands, resulting in a low-Φ_e contact. It is worthy to note that Φ_e becomes negative for the field smaller than 6 V/nm, which means that the Fermi level is above the CBM of penta-graphene, turning this contact into an Ohmic one. In this circumstance, electrons in graphene can spontaneously get injected into the penta-graphene layer, inducing an n-type doping of the penta-graphene channel. A previous experiment shows that a high bias (parallel to graphene) would lead to a breakdown in graphene-based devices.[40] However, the voltage applied in our study is perpendicular to the PG/G heterojunction, and the range of the electric field is comparable to that in previous studies, such as metal/h-BN/graphene[38] and phosphorene/graphene[18] systems. Thus, we believe that the PG/G heterojunction can withstand the electric field in this range.

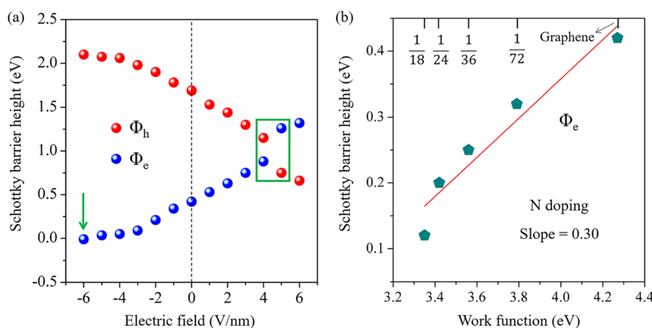

FIG. 5. (a) Evolution of the Schottky barrier heights as a function of the external electric field. (b) Variation of the Schottky barrier height of penta-graphene on the top of N-doped graphene.

We then show another approach to tune Φ_{SB}. According to the Schottky-Mott rule ($\Phi_e = W - E_{ea}$ and $\Phi_h = E_{ip} - W$), Φ_{SB} is related to the metal work function (W), which is equal to the difference between the Fermi level and the vacuum level. Therefore, by increasing or decreasing the number of electrons in the metal, the work function will be changed accordingly due to changes in the Fermi energy. Since the PG/G heterojunction possesses an n-type Φ_{SB}, we hope to obtain an enhanced device performance by reducing Φ_e. As we know, nitrogen is right next to carbon in the periodic table, and thus, the system will gain an electron by replacing a C atom with a nitrogen one, leading to a small W. In the PG/G contact, the supercell of graphene contains 72 carbon atoms. To confirm our conjecture, we substitute C atoms with 1, 2, 3, and 4 N atoms (structures can be seen in Fig. S5 in the supplementary material). We optimize the geometries of the heterostructures and calculate the Fermi level of these doped graphene layers. As expected, we observe that the Fermi level increases with the increasing doping concentration [see Fig. 5(b)], implying that nitrogen doping can effectively change the work functions. We then use the N-doped graphene layer as the electrode and calculate Φ_{SB} of these systems. The partial DOS of N-doped PG/G heterojunctions is given in the supplementary material. Figure 5(b) clearly shows that nitrogen doping significantly reduces Φ_e and leads to a small Φ_e value of 0.12 eV when the doping concentration is 1/18. We linearly fit these points in Fig. 5(b), obtaining a slope of -0.43, which implies that Fermi level pinning exists in these heterojunctions. It was demonstrated that the interface dipole is one of the main reasons for the Fermi level pinning.[22] The averaged charge density difference of the PG/G heterojunction, defined as $\Delta\rho = \rho$(heterojunction) - ρ(metal) - ρ(semiconductor), is plotted in Fig. S7 in the supplementary material. One can see that the charge redistribution is not symmetric between the two layers, leading to the formation of the interface dipole. Note that to keep the hexagonal lattice of graphene, the maximum N-doping concentration cannot exceed 33.3%.[41] In our study, the highest N concentration is 1/18 (5.56%), which is achievable in experiments.

From Table I, one can see that the PG/G heterojunction can be modeled by using different supercells. One may wonder how sensitive the calculated results are to the supercell size. Thus, we have also carried out additional calculations for Case 2 following the same procedure as Case 1. The main results are found to be consistent with each other, which confirms that our heterojunction model is reliable. Details can be found in the supplementary material.

In summary, we have studied the vdW heterojunction composed of penta-graphene and graphene. We used our in-house code to build the heterostructure model with a negligible

lattice mismatch strain and demonstrated that the PG/G heterojunction is energetically and thermally stable by calculating the binding energy and performing the AIMD simulation. Electronic structure analysis shows that (1) the intrinsic electronic properties of the isolated penta-graphene and graphene are preserved after being stacked together and a hybridized state appears at the valence band edge of penta-graphene, which is induced by the interaction between the p_z orbitals of penta-graphene and the π clouds in graphene; (2) there is a negative band bending at the lateral interface between the PG/G heterostructure and the freestanding penta-graphene, indicating an electron transfer from the stacked system to the channel material; (3) the Schottky barrier shows that an n-type character as the Fermi level of the PG/G heterojunction is closer to the CBM of penta-graphene; and (4) it is possible to tune the Schottky barrier by electrostatic gating or nitrogen doping graphene. We found that an Ohmic contact can be achieved under a negative field of 6 V/nm and a low-Φ_e can be realized by using the N-doped graphene as the electrode. These findings are very important for the exploration of penta-graphene in future device applications.

See supplementary material for more information on the stability and structural and electronic properties of PG/G heterostructures.

This work was partially supported by grants from the National Natural Science Foundation of China (NSFC-51471004) and the National Key Research and Development Program of China (2016YFE0127300). The calculations were carried out at the High Performance Computing Platform of CAPT at Peking University, China.

[1]K. Novoselov, D. Jiang, F. Schedin, T. Booth, V. Khotkevich, S. Morozov, and A. Geim, Proc. Natl. Acad. Sci. U.S.A. **102**, 10451 (2005).
[2]X. Qian, Y. Wang, W. Li, J. Lu, and J. Li, 2D Mater. **2**, 032003 (2015).
[3]K. S. Novoselov, A. K. Geim, S. V. Morozov, D. Jiang, Y. Zhang, S. V. Dubonos, I. V. Grigorieva, and A. A. Firsov, Science **306**, 666 (2004).
[4]A. K. Geim, Rev. Mod. Phys. **83**, 851 (2011).
[5]K. Novoselov, Rev. Mod. Phys. **83**, 837 (2011).
[6]F. Schwierz, Nat. Nanotechnol. **5**, 487 (2010).
[7]Q. H. Wang, K. Kalantar-Zadeh, A. Kis, J. N. Coleman, and M. S. Strano, Nat. Nanotechnol. **7**, 699 (2012).
[8]B. Radisavljevic, A. Radenovic, J. Brivio, I. V. Giacometti, and A. Kis, Nat. Nanotechnol. **6**(3), 147 (2011).
[9]L. Li, Y. Yu, G. J. Ye, Q. Ge, X. Ou, H. Wu, D. Feng, X. H. Chen, and Y. Zhang, Nat. Nanotechnol. **9**, 372 (2014).
[10]S. Zhang, J. Zhou, Q. Wang, X. Chen, Y. Kawazoe, and P. Jena, Proc. Natl. Acad. Sci. U.S.A. **112**, 2372 (2015).
[11]A. K. Geim and I. V. Grigorieva, Nature **499**, 419 (2013).
[12]K. Novoselov, A. Mishchenko, A. Carvalho, and A. C. Neto, Science **353**, aac9439 (2016).
[13]W. Yu, Z. Zhu, S. Zhang, X. Cai, X. Wang, C.-Y. Niu, and W.-B. Zhang, Appl. Phys. Lett. **109**, 103104 (2016).
[14]V. D. S. O. Ganesan, J. Linghu, C. Zhang, Y. P. Feng, and L. Shen, Appl. Phys. Lett. **108**, 122105 (2016).
[15]L. Britnell, R. Gorbachev, R. Jalil, B. Belle, F. Schedin, A. Mishchenko, T. Georgiou, M. Katsnelson, L. Eaves, and S. Morozov, Science **335**, 947 (2012).
[16]C.-J. Shih, Q. H. Wang, Y. Son, Z. Jin, D. Blankschtein, and M. S. Strano, ACS Nano **8**, 5790 (2014).
[17]L. Yu, Y.-H. Lee, X. Ling, E. J. Santos, Y. C. Shin, Y. Lin, M. Dubey, E. Kaxiras, J. Kong, and H. Wang, Nano Lett. **14**, 3055 (2014).
[18]J. Padilha, A. Fazzio, and A. J. da Silva, Phys. Rev. Lett. **114**, 066803 (2015).
[19]C. Si, Z. Lin, J. Zhou, and Z. Sun, 2D Mater. **4**, 015027 (2016).
[20]M. Neek-Amal, A. Sadeghi, G. Berdiyorov, and F. Peeters, Appl. Phys. Lett. **103**, 261904 (2013).
[21]A. Dimoulas, P. Tsipas, A. Sotiropoulos, and E. Evangelou, Appl. Phys. Lett. **89**, 252110 (2006).
[22]Y. Liu, P. Stradins, and S.-H. Wei, Sci. Adv. **2**, e1600069 (2016).
[23]G. Kresse and J. Furthmüller, Phys. Rev. B **54**, 11169 (1996).
[24]G. Kresse and D. Joubert, Phys. Rev. B **59**, 1758 (1999).
[25]P. E. Blöchl, Phys. Rev. B **50**, 17953 (1994).
[26]J. P. Perdew, K. Burke, and M. Ernzerhof, Phys. Rev. Lett. **77**, 3865 (1996).
[27]J. Klimeš, D. R. Bowler, and A. Michaelides, J. Phys.: Condens. Matter **22**, 074203 (2010).
[28]J. Klimeš, D. R. Bowler, and A. Michaelides, Phys. Rev. B **83**, 195131 (2011).
[29]H. J. Monkhorst and J. D. Pack, Phys. Rev. B **13**, 5188 (1976).
[30]H.-P. Komsa and A. V. Krasheninnikov, Phys. Rev. B **88**, 085318 (2013).
[31]A. Zur and T. McGill, J. Appl. Phys. **55**, 378 (1984).
[32]G. Graziano, J. Klimeš, F. Fernandez-Alonso, and A. Michaelides, J. Phys.: Condens. Matter **24**, 424216 (2012).
[33]S. Nosé, J. Chem. Phys. **81**, 511 (1984).
[34]A. K. Geim and K. S. Novoselov, Nat. Mater. **6**, 183 (2007).
[35]J. Kang, W. Liu, and K. Banerjee, Appl. Phys. Lett. **104**, 093106 (2014).
[36]K. Gong, L. Zhang, W. Ji, and H. Guo, Phys. Rev. B **90**, 125441 (2014).
[37]N. Kaushik, A. Nipane, F. Basheer, S. Dubey, S. Grover, M. M. Deshmukh, and S. Lodha, Appl. Phys. Lett. **105**, 113505 (2014).
[38]M. Bokdam, P. A. Khomyakov, G. Brocks, Z. Zhong, and P. J. Kelly, Nano Lett. **11**, 4631 (2011).
[39]B. Sachs, L. Britnell, T. Wehling, A. Eckmann, R. Jalil, B. Belle, A. Lichtenstein, M. Katsnelson, and K. Novoselov, Appl. Phys. Lett. **103**, 251607 (2013).
[40]A. Barreiro, F. Börrnert, M. H. Rümmeli, B. Büchner, and L. M. K. Vandersypen, Nano Lett. **12**, 1873 (2012).
[41]Z. Shi, A. Kutana, and B. Yakobson, J. Phys. Chem. Lett. **6**(1), 106 (2015).